Fault-Tolerant Independent Pole Control Scheme of Zigzag MMC for Bipolar MVDC Distribution Systems

Dong-Joon Kim, *Graduate Student Member, IEEE*, Jaeyeon Park, *Graduate Student Member, IEEE*, Yeonjoo Hong, *Member, IEEE*, and Shenghui Cui, *Senior Member, IEEE*

***Abstract*—This article presents a fault-tolerant independent pole control scheme for a zigzag modular multilevel converter (MMC) targeting bipolar medium-voltage direct-current (MVDC) distribution systems. An MMC which adopts a zigzag transformer as an ac grid interface transformer, namely zigzag MMC, has inherent bipole operation capability with unbalanced loads of positive and negative poles on the dc side. Nevertheless, this topology has not been thoroughly investigated for its ability to maintain independent control of each pole in the case of a fault in the other. With a conventional MMC control which relies on normal operation of both poles, a fault in a single pole is likely to impact the overall operation of the converter. To tackle this problem, the proposed control scheme separates the arm current controllers and energy balancing controllers within upper and lower arms individually. Additional power reference coupling is introduced to indirectly inject circulating currents when both poles are healthy like the conventional MMC. When a single pole fault occurs, a seamless energy-balancing mode transition can be achieved by modifying inputs to current reference calculators. An ac-side single line-to-ground (SLG) fault ride through strategy can also be integrated without compromising the independence of both poles. A point-to-point zigzag-MMC based bipolar MVDC distribution system is tested by controller hardware-in-the-loop est setup. The test results under single pole-to-ground fault and ac SLG fault validate the effectiveness of the proposed control scheme. Moreover, experimental results using a downscaled MMC prototype and a zigzag transformer further demonstrate the performance of the proposed control scheme under abrupt single-pole blocking and ac SLG fault conditions.**

Received 23 August 2025; revised 1 December 2025; accepted 11 January 2026. Date of publication 16 January 2026; date of current version 20 March 2026. This work was supported in part by the Korea Institute of Energy Technology Evaluation and Planning (KETEP), Ministry of Climate, Energy and Environment (MCEE) of South Korea under Grant 20225500000130 (20MW MMC-based MVDC Converter Station) and in part by the Technology Innovation Program (or Industrial Strategic Technology Development Program under Grant RS-2024-00432085, Development of Control System for High Power Medium-Voltage Drive based on Modular Multilevel Converter) funded by the Ministry of Trade, Industry and Energy (MOTIE) of South Korea. Recommended for publication by Associate Editor B. Li. *(Corresponding author: Shenghui Cui.)*

Dong-Joon Kim, Jaeyeon Park, and Shenghui Cui are with the Department of Electrical and Computer Engineering and SNU Electric Power Research Institute, Seoul National University, Seoul 08826, South Korea (e-mail: totorokdj@snu.ac.kr; ok6530@snu.ac.kr; cuish@snu.ac.kr).

Yeonjoo Hong is with HD Korea Shipbuilding & Offshore Engineering Company, Ltd, Gyeonggi-do 13553, South Korea (e-mail: yeonjoo.hong@hd.com).

Color versions of one or more figures in this article are available at https://doi.org/10.1109/TPEL.2026.3655014.

Digital Object Identifier 10.1109/TPEL.2026.3655014

***Index Terms*—Bipole, dc distribution, fault ride through (FRT), modular multilevel converter (MMC), pole-to-ground (PtG) fault, single line-to-ground (SLG) fault, zigzag transformer.**

NOMENCLATURE

x	Subscript indicating phase a, b, or c.
$\sum_x$	Sum over the three phases.
$\alpha\beta0$	Subscript indicating Clarke-transformed quantity. (0 indicates the zero-sequence component.)
dq	Subscript indicating a quantity transformed into the synchronous (dq) reference frame.
u	Subscript indicating upper arm quantity.
l	Subscript indicating lower arm quantity.
$^+$	Superscript indicating positive-sequence component.
$^-$	Superscript indicating negative-sequence component.
*	Superscript indicating reference value.
E_{xu}	Total energy stored in all submodule capacitors in the corresponding upper arm.
E_{xl}	Total energy stored in all submodule capacitors in the corresponding lower arm.
i_{xu}	Upper arm currents.
i_{xl}	Lower arm currents.
$i_{dc,u}$	Positive-pole current; equivalent to the sum of upper arm currents.
$i_{dc,l}$	Negative-pole current; equivalent to the sum of lower arm currents.
$i_{xs,u}$	Upper arm current excluding zero-sequence component flowing toward the ac side of MMC.
$i_{xs,l}$	Lower arm current excluding zero-sequence component flowing toward the ac side of MMC.
$i_{xu,dc}$	Non zero-sequence dc component of upper arm currents whose sum over three phases is zero.
$i_{xl,dc}$	Non zero-sequence dc component of lower arm currents whose sum over three phases is zero.
v_{xs}	Phase voltage of secondary side of a transformer.
i_{xs}	Phase current of secondary side of a transformer.
i_{xp}	Phase current of primary side of a transformer.
$V_{dc,u}$	Rated positive-pole voltage.
$V_{dc,l}$	Rated negative-pole voltage.
θ^+	Phase angle used to align v_{xs}^+ with the q-axis in the synchronous reference frame.

I. Introduction

THE dc distribution is an upcoming and promising solution due to the fact that it can flexibly integrate various energy storage systems, renewable energy sources, and dc loads like electric vehicle charging [1]. In medium-voltage direct current (MVDC) distribution systems, the system voltage level typically reaches dozens of kV. As a result, conventional voltage-source converter (VSC) topologies, such as two-level or three-level converters, may not be directly applicable for interfacing existing ac grids and dc networks. Considering these aspects, a modular multilevel converter (MMC) can be a suitable candidate taking advantage of its high scalability and superior harmonic performance [2].

There are several existing options for the system configuration adopting the MMC topology [3], as depicted in Fig. 1. Although a symmetrical monopole configuration, as shown in Fig. 1(a), seems a simple and cost-effective solution, it cannot provide power redundancy if a fault occurs in a single pole. On the other hand, a bipole configuration with a dedicated metallic return (DMR), as shown in Fig. 1(b), ensures higher availability compared to monopole configurations, by independently controlling two asymmetrical monopoles. Regarding that one of the key factors of the distribution system is availability, the bipole configuration is a reasonable way to set up the MVDC distribution system [4].

In [5], an MMC with a zigzag transformer, namely a zigzag MMC, was first proposed for cost-effective bipolar MVDC distribution systems. Even though this circuit-wise configuration resembles the symmetrical monopole configuration since it consists of a single MMC and a single grid interface transformer, the bipole operation of both poles can be available by applying zigzag winding to the secondary side of the transformer. Nevertheless, only unbalanced load condition of both poles on the dc side was considered in [5], where the normal operation with healthy condition of both poles of the entire MMC is assumed. Adopting the same concept proposed in [5], a seamless mode transition scheme from the bipole operation to the asymmetrical monopole operation is proposed in [6]. However, only the failure of all redundant submodules in a certain arm is assumed in [6], when the MMC is still fully under control and a pre-planned mode transition can be initiated deliberately. This topology still lacks a comprehensive investigation of control strategies to tackle with various contingency fault scenarios, e.g., a pole-to-ground (PtG) short-circuit fault.

A key requirement for bipole operation is that each pole remains independently controllable, regardless of fault and trip in the other pole. However, a well-established control scheme for a single MMC relies on symmetric components between both poles [2], which means that a fault in a single pole is likely to impact the overall operation of the converter. Several approaches have been investigated to realize the independent pole control of a single MMC [7], [8], [9]. In [7], capacitor voltage control and arm current control were established for each pole of MMC. Since negative-sequence current injection into the ac side is always necessary for the balancing of submodule capacitor voltages, the control scheme proposed in [7] is not the best option under unbalanced ac voltages [10]. Asymmetrical monopole operation strategy for half-bridge submodule based MMC considering dc pole imbalance was proposed in [8]. Although this strategy works well if both poles are under normal operation, fault scenarios of a single pole were not addressed in [8]. An independent pole control scheme of hybrid MMC was presented in [9]. Comprehensive analysis on the control scheme in [9] was handled regarding capacitor energy, unbalanced dc pole voltage, and operating region. Moreover, PtG fault ride through (FRT) strategy was investigated and simulations results covered other fault conditions including dc pole-to-pole (PtP) and three-phase ac fault. Nevertheless, the control method in [9] still assumes that both poles of the MMC are fully controllable. Also, ac single line-to-ground (SLG) fault was not considered and the control scheme in [9] assumed the same dc pole currents due to the saturation of the transformer, whereas the zigzag transformer can handle unbalanced dc pole currents [11]. Therefore, the control method proposed in [9] only tackles with the case of unbalanced pole voltages, while it cannot fully enable bipole operation, where the unbalanced pole currents should be addressed. Table I provides a comprehensive summary of the comparison, highlighting the limitations of existing studies related to the bipole operation scheme using a single MMC.

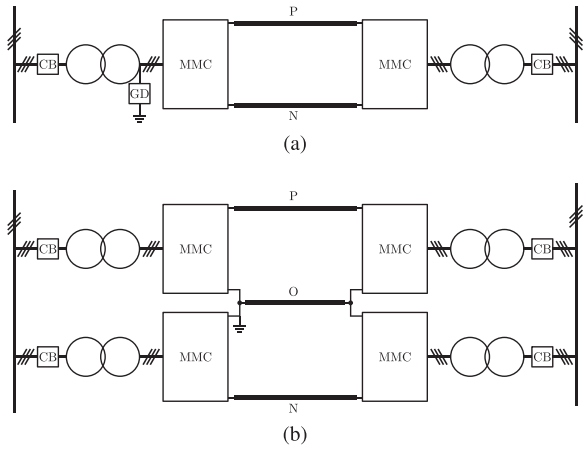

Fig. 1. MMC-based system configurations. (The symbol CB denotes a circuit breaker.) (a) Symmetrical monopole. (The symbol GD denotes a grounding device.) (b) Bipole with a dedicated metallic return.

Regarding aforementioned aspects, a novel independent pole control for a single zigzag MMC is proposed in this article. The key ideas and contributions of this work are summarized as follows.

1) Upper and lower arm currents are controlled separately including each pole current. Instead of only using negative-sequence ac-side current for energy balancing, the proposed scheme can indirectly inject circulating current as in the conventional control method of an MMC [12] by coupling upper and lower balancing controller power references in a simple manner when both poles are healthy.
2) A seamless power reference transition, which immediately decouples the upper and lower balancing controllers, is proposed in this article. As a result, the proposed control

TABLE I
COMPARISON OF EXISTING BIPOLE OPERATION SCHEMES FOR A SINGLE MMC

Ref.	Topology	Operation Capability with Unbalanced Pole Currents	Control Scheme of Both Poles	AC SLG Fault	Single-Pole Fault
[7]	Full-bridge MMC	×	Independent	△[2]	–[3]
[8]	Half-bridge MMC (Dedicated star-point reactor)	✓	Dependent[1]	–[3]	–[3]
[9]	Hybrid MMC	×	Independent	–[3]	△[4]
[5],[6]	Half-bridge zigzag MMC	✓	Dependent	–[3]	△[4]
This work	Half-bridge zigzag MMC	✓	Independent	✓	✓

[1] Relies on the conventional MMC modeling.
[2] Undesired negative-sequence phase currents for energy balancing.
[3] Not discussed.
[4] Only available when both poles are controllable.

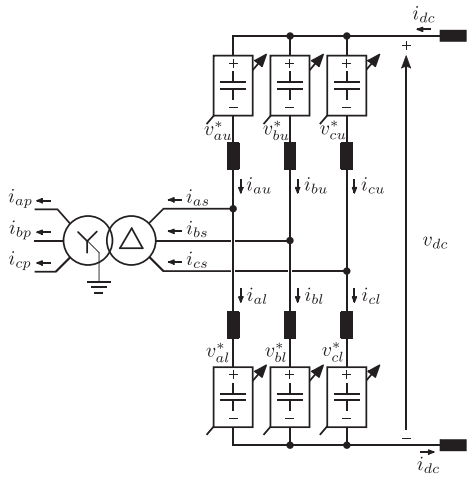

Fig. 2. Schematic of the conventional MMC.

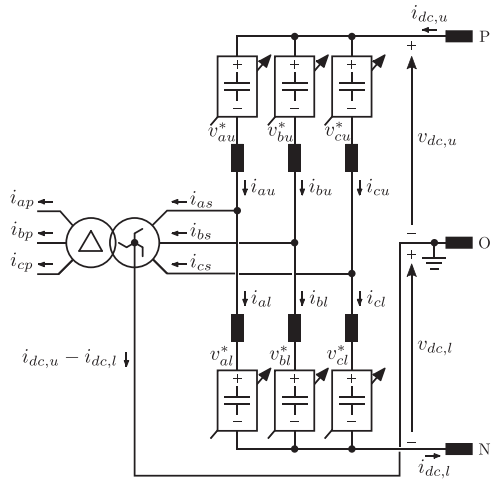

Fig. 3. Schematic of the zigzag MMC.

scheme enables the continuous operation of healthy pole even if the fault occurs in the other pole, thereby fully utilizing the bipole operation capability of a single zigzag MMC.

3) An SLG ac fault in the case of point-to-point system is considered in the proposed independent pole control scheme. An SLG ac FRT strategy can be integrated while preserving the independent pole control capability. Feedforward terms under unbalanced ac conditions are also utilized in the proposed control scheme.

The effectiveness of the proposed control scheme is validated with a controller hardware-in-the-loop (CHIL) test system utilizing real-time simulators. A point-to-point bipolar MVDC distribution system is configured using two real-time simulators, each of which emulates a single zigzag MMC station. Experimental results using a downscaled MMC prototype and a zigzag transformer also further validate the proposed control scheme.

II. CIRCUIT OF ZIGZAG MMC

Unlike the conventional MMC configuration shown in Fig. 2, the zigzag MMC utilizes a delta-zigzag transformer for ac-grid connection, as depicted in Fig. 3. The secondary-side windings

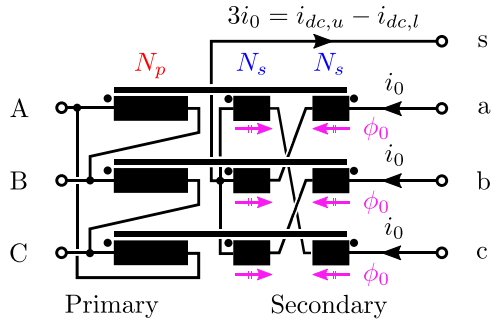

Fig. 4. Zigzag transformer winding.

of the transformer are connected in a zigzag manner, as shown in Fig. 4, such that the magnetic fluxes induced by the zero-sequence winding current are canceled out in each core. This is attributed to the fact that the magnetomotive forces generated by both sets of secondary-side windings on the same core are with the same magnitudes but opposite polarities as indicated by the dot convention. In addition, the star point of the secondary side is connected to the neutral cable conductor, namely the DMR, of the bipolar MVDC distribution systems. The neutral

TABLE II
COMPARISON OF CONVENTIONAL BIPOLAR SYSTEM AND ZIGZAG MMC

	Conventional Bipolar System	Zigzag MMC
Number of MMC	2	1
Number of Transformer	2	1
Number of Air-core Arm Reactor	12	6
Transformer Insulation	ac and dc	ac only
Cost / Footprint	High	Low
Reliability	Superior	High
Main Application	HVDC	MVDC

conductor can be grounded solidly or with an impedance depending on the application requirements. With this configuration, the zigzag MMC can operate continuously without saturation of the transformer, even if a zero-sequence dc winding current flows via the star point in the case of pole-current imbalance. Furthermore, bipole operation of the converter can be achieved without penalty of increased voltage or current stress on the components. Validity of the concept was verified by simulations and experiments regarding unbalanced dc loads between both poles in [5].

A. Comparison With Conventional Bipolar Systems

A typical configuration of conventional bipolar systems requires two MMCs and two transformers for interfacing a single ac grid as shown in Fig. 1(b). Therefore, each transformer must endure not only the rated ac voltage, but also the half of the rated dc voltage against ground potential in terms of insulation. On the other hand, only a single transformer is used in the case of the zigzag MMC and this transformer only has to endure the rated ac voltage if the star point of the secondary side is grounded. This feature alleviates the difficulty of transformer insulation design.

In addition, different from the conventional bipolar MVDC stations in Fig. 1(b), the zigzag MMC only requires one transformer and one MMC, which can significantly reduce the cost and footprint of the converter station. However, from the perspective of system reliability, the risk associated with a transformer failure increases due to the reduced redundancy of transformers. Nevertheless, since the typical lifetime of a distribution transformer is estimated to be around 10–20 years [13], [14], the reduction in the number of transformers would not significantly affect the overall system reliability in MVDC applications. This trade-off between cost, reliability, and insulation requirements is summarized in Table II.

One might argue that if the star point of the transformer is grounded, the conventional third-harmonic zero-sequence voltage injection method for enlarging modulation index cannot be utilized in the zigzag MMC. Although this may be a critical drawback for high-voltage direct-current (HVDC) transmission systems where a large number of submodules are needed, zigzag MMC is still an attractive option for MVDC applications, where the number of submodules is not much high.

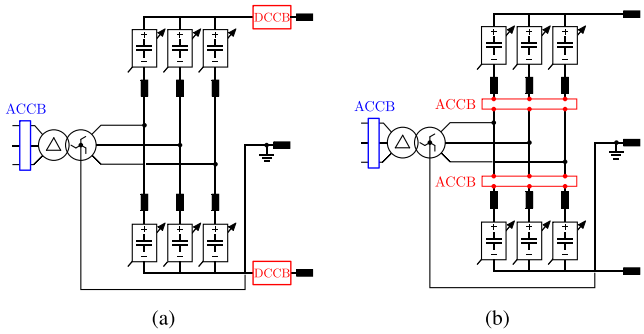

Fig. 5. DC-side short-circuit fault clearing strategies for zigzag MMC. (a) Using DCCBs. (b) Using ACCBs.

B. DC-Side Fault Clearing Strategies for Zigzag MMC

A number of topologies and operation strategies have been developed for HVDC transmission systems, to ensure continuous and seamless system operation under faults, regardless of the system configuration. Especially for PtP and PtG faults on the dc sides, it is well known that an MMC which consists of sufficient full-bridge submodules provides FRT capability [15], [16]. Although concepts proposed in [15], [16] are applicable to MVDC distribution systems, these concepts are undesired for MVDC applications due to high losses of full-bridge submodules and high capital costs [17]. Therefore, this article mainly focuses on a half-bridge submodule based MMC, which needs circuit breakers for dc-side fault clearing.

As shown in Fig. 5(a), two dc circuit breakers (DCCBs) can be installed at both poles to deal with corresponding dc-side faults. Although it is common in MVDC power systems to use DCCBs for fast protection, DCCBs are costly and their control is complex in practice [18]. On the other hand, two ac circuit breakers (ACCBs) can be utilized instead of DCCBs as shown in Fig. 5(b). Half-bridge submodules are typically equipped with thyristors and bypass switches, which are activated during dc short-circuit faults to protect the power semiconductor devices from fault currents [19], [20], [21]. In consequence, the faulty pole then behave as a half-wave rectifier where zero-crossing points of arm currents are naturally present. With these zero-crossing points, the associated ACCB can be tripped but much slowly than the DCCBs.

It is important to note that an ACCB should be also installed in the primary side of the transformer for both cases, such that the transformer can be de-energized from the grid by tripping corresponding ACCB. As a result, unlike the conventional bipolar system as shown in Fig. 1(b), the number of installed ACCB increases when the zigzag MMC adopts the dc-side fault clearing strategy using ACCBs, as shown in Fig. 5(b). Both fault-clearing options are considered in the PtG fault simulation described in Section VI.

III. MODELING OF ZIGZAG MMC

This section presents a reformulated perspective on MMC modeling to facilitate understanding of the proposed control scheme. The following subsections compare conventional and

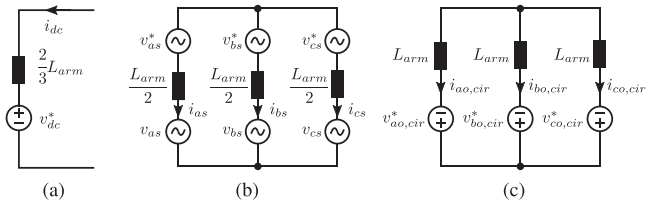

Fig. 6. Equivalent circuits of the conventional MMC modeling. (a) DC-side current equivalent circuit. (b) AC-side current equivalent circuit. (c) Circulating current equivalent circuit.

reformulated MMC models with respect to arm current and energy balancing control, respectively.

A. Arm Current

Following the conventional MMC modeling [2], [12], upper and lower arm currents are written as

$$i_{xu} = \frac{1}{3}i_{dc} + \frac{1}{2}i_{xs} + i_{xo,cir} \tag{1}$$

$$i_{xl} = \frac{1}{3}i_{dc} - \frac{1}{2}i_{xs} + i_{xo,cir} \tag{2}$$

where i_{dc} denotes dc-side current of MMC; i_{xs} denotes ac-side current of MMC; and $i_{xo,cir}$ denotes circulating current, which is not present on both ac and dc sides of MMC. Each equivalent circuit based on the conventional MMC modeling is depicted in Fig. 6. The dc-side current, ac-side current, and the circulating current can be modeled and controlled independently as indicated by Fig. 6. Therefore, in the conventional MMC control, the current control is executed based on the independent control of dc-link current, ac-side current, and circulating current rather than controlling upper and lower arm currents directly as control targets. As these expressions indicate that upper and lower arm currents are coupled, a current control scheme based on this arm current modeling is effective only when the entire converter operates normally. Also, it is worth noting that equal pole currents are assumed, since the conventional MMC cannot operate under pole-current imbalance condition.

However, when the case of unbalanced pole currents is considered, upper and lower arm currents can be reconstructed alternatively as

$$i_{xu} = \frac{1}{3}i_{dc,u} + i_{xs,u} \tag{3}$$

$$i_{xl} = \frac{1}{3}i_{dc,l} - i_{xs,l}. \tag{4}$$

Note that the zero-sequence dc components are defined individually for positive and negative poles compared to the conventional modeling. These definitions imply that the unbalanced pole currents can flow through the secondary side of the transformer thanks to the feature of the zigzag winding arrangement. Each equivalent circuit of the generalized zigzag MMC modeling is shown in Fig. 7, and independent current control between both poles can be achieved based on these equivalent circuits.

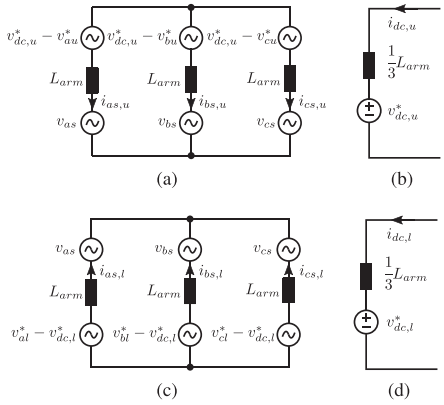

Fig. 7. Equivalent circuits of the generalized zigzag MMC modeling. (a) Upper arm AC-side equivalent circuit. (b) Upper arm DC-side equivalent circuit. (c) Lower arm AC-side equivalent circuit. (d) Lower arm DC-side equivalent circuit.

Secondly, $i_{xs,u}$, $i_{xs,l}$ are decomposed into three components as

$$i_{xs,u} = i^{+}_{xu} + i^{-}_{xu} + i_{xu,dc} \tag{5}$$

$$i_{xs,l} = i^{+}_{xl} + i^{-}_{xl} + i_{xl,dc}. \tag{6}$$

The purpose of this modeling is to fully exploit circulating current components for arm energy balancing, similarly to the control scheme proposed in [12]. Although circulating currents are not directly defined in (3) and (4), it is important to note that they can still be indirectly injected if the following conditions are met.

1) The sum of the currents over the three phases should be zero in order not to affect the dc side of MMC. Therefore, a portion of $i_{xs,u}$ and $i_{xs,l}$ can contribute to the circulating current.
2) A specific component of $i_{xs,u}$ and $i_{xs,l}$ should have the same magnitude but opposite signs in order not to affect the ac side of MMC; e.g., $i^{-}_{xu} = -i^{-}_{xl}$.

These conditions are appropriately employed in the proposed control scheme via power reference coupling, which is described in Section IV. This coupling is enabled when both poles are healthy so that unnecessary continuous negative-sequence current injection into the ac side can be avoided unlike in [7]. Also, the dc components of the circulating currents can be injected using $i_{xu,dc}$ and $i_{xl,dc}$, which provides advantages such as lower capacitor voltage ripple and balanced ac-side currents during ac SLG FRT [10].

B. Arm Energy Balancing Problem

An arm energy balancing control problem of MMC has a total of six degrees of freedom (DOFs) to address, corresponding to the control of the energy of the six arms at their rated values [22]. These DOFs can be grouped into the following equivalent balancing problems [12]:

$$\begin{cases} \sum_x (E_{xu} + E_{xl}) = 6E_{rated} \\ E_{au} + E_{al} = E_{bu} + E_{bl} = E_{cu} + E_{cl} \\ E_{au} - E_{al} = E_{bu} - E_{bl} = E_{cu} - E_{cl} = 0. \end{cases} \tag{7}$$

This grouping also shares the same framework as that of horizontal and vertical balancing [23]. From (7), it can be noticed that upper and lower arm energies are coupled. In consequence, an arm energy balancing control based on these balancing problems is valid only when the entire converter operates normally.

Instead, these problems can be reformulated as follows:

$$\sum_x E_{xu} = 3E_{rated} \tag{8}$$

$$E_{au} = E_{bu} = E_{cu} \tag{9}$$

$$\sum_x E_{xl} = 3E_{rated} \tag{10}$$

$$E_{al} = E_{bl} = E_{cl}. \tag{11}$$

Based on these reformulated balancing problems, energies of upper and lower arms can be separately controlled. Energy balancing controllers to handle these balancing problems are described in detail in Section IV.

IV. Proposed MMC Independent Pole Control

The control strategy of zigzag MMC was already discussed in [5], considering unbalanced dc loads. However, like other MMC control strategies [2], it assumes the normal operation of both upper and lower arms. Although this strategy is effective under normal operation conditions where both poles are healthy and fully under control, the whole converter cannot sustain continuous operation in the case of a single pole failure because this assumption is no longer valid.

Unlike the conventional MMC arm capacitor energy balancing control schemes [12], [22], [23], the proposed control strategy independently handles energy balancing for upper and lower arms. By separating upper and lower arm energy balancing controllers, each pole can be operated regardless of failure of the other pole.

A. Arm Current Control

To independently control upper and lower arm currents, two separate arm current controllers are adopted in this article.

Applying the superposition principle, the total of four arm current components can be controlled with the following arm output voltage references:

$$v^*_{xu} = \underbrace{v^*_{dc,u}}_{\text{DC side}} \underbrace{- v^{+*}_{xu} - v^{-*}_{xu} - v^*_{xu,dc}}_{\text{PIR control}} \tag{12}$$

$$v^*_{xl} = \underbrace{v^*_{dc,l}}_{\text{DC side}} \underbrace{+ v^{+*}_{xl} + v^{-*}_{xl} + v^*_{xl,dc}}_{\text{PIR control}}. \tag{13}$$

$v^*_{dc,u}$, $v^*_{dc,l}$ indicate the pole-voltage references, which are used to control the pole currents in the inverter mode and the pole voltages in the rectifier mode. To control remaining arm currents accordingly, proportional-integral-resonant (PIR) controllers [5] are implemented for both poles in the stationary reference frame. Each sensed secondary-side phase voltage of the transformer v_{xs} is also used for voltage feedforward for both current controllers to enhance current-control dynamics. In addition, dual second-order generalized integrator is implemented to extract both positive-sequence components v^+_{xs} and negative-sequence components v^-_{xs} from sensed phase voltages in order to deal with the unbalanced ac grid condition. With the extracted positive-sequence phase voltages, synchronous reference frame phase-locked loop (SRF-PLL) is adopted to track instantaneous phase angles for transforming dq-axes current references into three-phase current references [24]. PIR controller gains are tuned based on the phase equivalent circuit of each arm as shown Fig. 7(a) and Fig. 7(c).

Overall current control schemes are depicted in Fig. 8. Note that the indirect-modulation scheme, which is described in [25], is used in this article for the accurate synthesis of the arm output voltage references.

B. Arm Energy Balancing Control

Equations (8) and (10) need 1 DOF each and (9) and (11) need 2 DOFs each, which can be mapped to 3 DOFs of the Clarke transformation, respectively [23]. Since each arm energy has both fundamental and twice-line-frequency energy ripples [26], two notch filters are applied in series to remove both types of ripples.

In order to control the arm capacitor energy, power references are generated with simple proportional-integral (PI) controllers considering control DOFs as shown in Fig. 8. Since v^{-*}_{xu}, v^{-*}_{xl}, $v^*_{xu,dc}$, $v^*_{xl,dc}$ are negligible during normal operation, averaged powers of upper and lower arms over one ac-side fundamental period are calculated using (3), (4), (12), and (13) as

$$P_{xu} = \underbrace{v^*_{dc,u}\frac{i_{dc,u}}{3} - v^{+*}_{xu}i^+_{xu}}_{\text{zero-sequence components}} + \underbrace{v^*_{dc,u}i_{xu,dc} - v^{+*}_{xu}i^-_{xu}}_{\alpha\beta \text{ components}} \tag{14}$$

$$P_{xl} = \underbrace{v^*_{dc,l}\frac{i_{dc,l}}{3} - v^{+*}_{xl}i^+_{xl}}_{\text{zero-sequence components}} - \underbrace{v^*_{dc,l}i_{xl,dc} - v^{+*}_{xl}i^-_{xl}}_{\alpha\beta \text{ components}}. \tag{15}$$

According to (14) and (15), sums of averaged upper arm and lower arm powers are deduced as

$$\sum_x P_{xu} = 3P_{0u} = v^*_{dc,u}i_{dc,u} - 3v^{+*}_{xu}i^+_{xu} \tag{16}$$

$$\sum_x P_{xl} = 3P_{0l} = v^*_{dc,l}i_{dc,l} - 3v^{+*}_{xl}i^+_{xl} \tag{17}$$

since the sum of $\alpha\beta$ components is zero. In the proposed control strategy, power references to achieve (8) and (10) are regulated using the ac-side active power by controlling positive-sequence currents.

When both poles are in the normal operation mode, power references, which realize balancing problems of (9) and (11), are coupled as follows:

$$P^*_{\alpha u,dc} = \frac{v^*_{dc,u}}{v^*_{dc,u} + v^*_{dc,l}}(P^*_{\alpha u} + P^*_{\alpha l}) \tag{18}$$

$$P^*_{\beta u,dc} = \frac{v^*_{dc,u}}{v^*_{dc,u} + v^*_{dc,l}}(P^*_{\beta u} + P^*_{\beta l}) \tag{19}$$

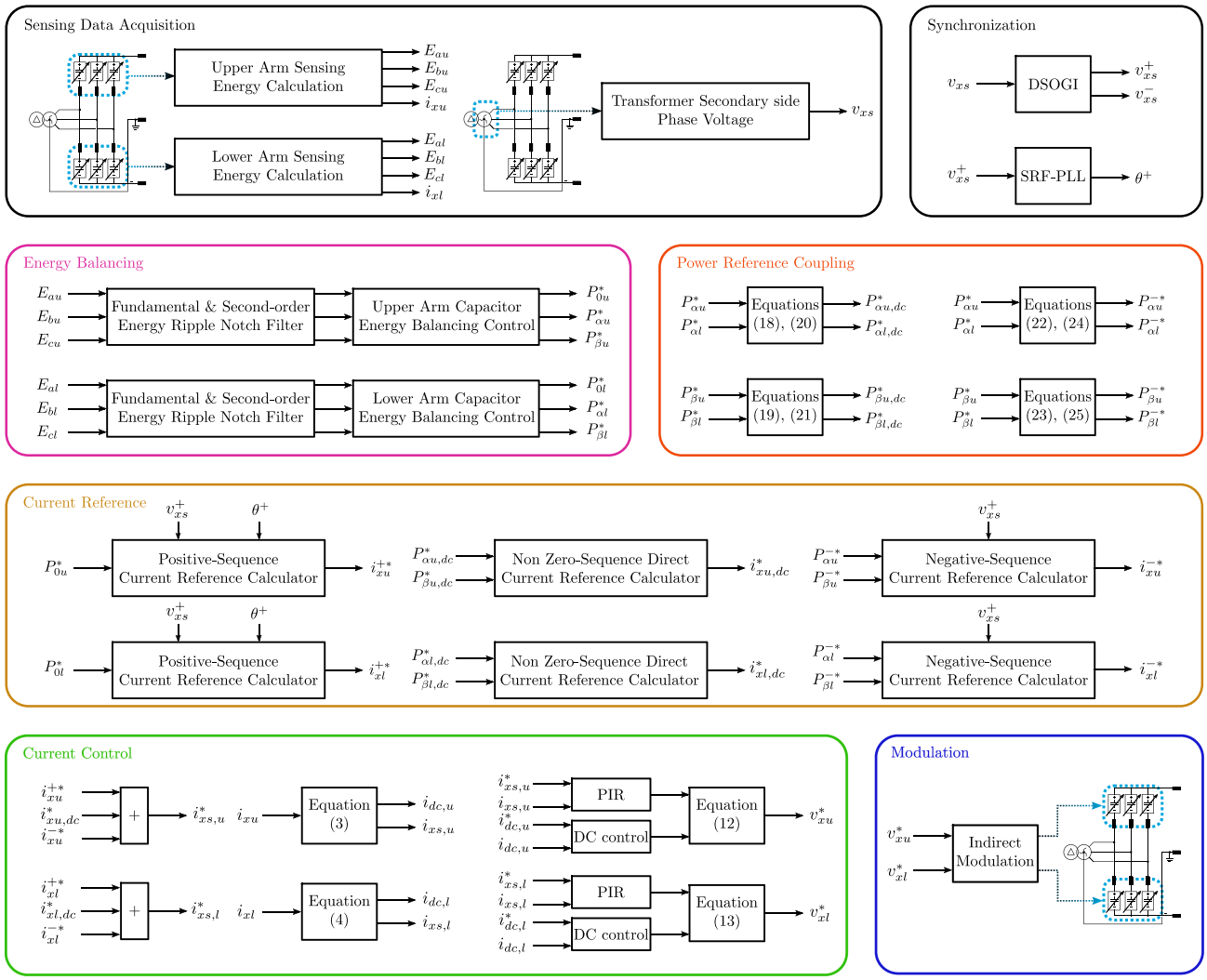

Fig. 8. Block diagram of the proposed MMC control scheme in the case of the inverter mode.

$$P^*_{\alpha l,dc} = \frac{v^*_{dc,l}}{v^*_{dc,u} + v^*_{dc,l}}(P^*_{\alpha u} + P^*_{\alpha l}) \tag{20}$$

$$P^*_{\beta l,dc} = \frac{v^*_{dc,l}}{v^*_{dc,u} + v^*_{dc,l}}(P^*_{\beta u} + P^*_{\beta l}) \tag{21}$$

$$P^{-*}_{\alpha u} = P^*_{\alpha u} - P^*_{\alpha u,dc} \tag{22}$$

$$P^{-*}_{\beta u} = P^*_{\beta u} - P^*_{\beta u,dc} \tag{23}$$

$$P^{-*}_{\alpha l} = P^*_{\alpha l} - P^*_{\alpha l,dc} \tag{24}$$

$$P^{-*}_{\beta l} = P^*_{\beta l} - P^*_{\beta l,dc}. \tag{25}$$

Then, $i_{xu,dc}$ and $i_{xl,dc}$ are selected to realize the power references in (18)–(21), while i^-_{xu} and i^-_{xl} are selected to realize the power references in (22)–(25).

Note that both positive-sequence and negative-sequence current references are derived using v^+_{xs} neglecting the voltage drops of arm inductors since both v^{+*}_{xu} and v^{+*}_{xl} consist of v^+_{xs}. Therefore, each current reference of upper and lower arms utilizes the same calculators, respectively, as shown in Fig. 8.

The detailed structures of the current reference calculators are depicted in Fig. 9. As shown in Fig. 9(a), the positive-sequence current references are derived from the q-axis current references, while v^+_{xs} is oriented to the q-axis.

To calculate the non zero-sequence dc current references, the power references in (18)–(21) are transformed into three-phase values and then they are divided by the pole voltages, as shown in Fig. 9(b). Therefore, the relationship between $i^*_{xu,dc}$ and $i^*_{xl,dc}$ is deduced as

$$i^*_{xu,dc} = -i^*_{xl,dc}. \tag{26}$$

Lastly, regarding the upper arm negative-sequence current reference calculator, the inputs to the calculator are formulated using the averaged power as

$$\begin{cases} P^{-*}_{\alpha u} = -\dfrac{V^+ I^-}{2}\cos\phi \\ P^{-*}_{\beta u} = -\dfrac{V^+ I^-}{2}\sin\phi \end{cases} \tag{27}$$

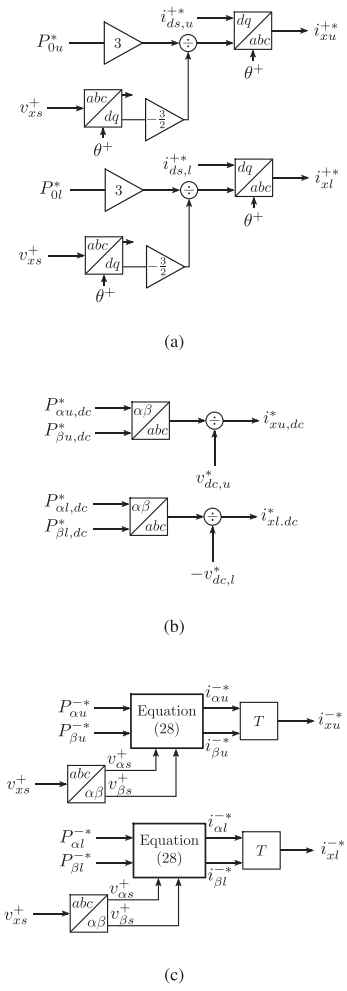

Fig. 9. Block diagrams of current reference calculators. (a) Positive-sequence current references. (b) Non zero-sequence DC current references. (c) Negative-sequence current references.

where V^+ denotes the magnitude of the v^+_{xs}; I^- denotes the magnitude of i^-_{xu}; and ϕ denotes the phase of the power references in the $\alpha\beta$-axes. In order to generate the corresponding current references, similar equations are used following a negative-sequence circulating current reference calculation scheme described in [12]

$$\begin{cases} i^{-*}_{\alpha u} = -2\dfrac{P^{-*}_{\alpha u}v^+_{\alpha s} - P^{-*}_{\beta u}v^+_{\beta s}}{V^{+2}} \\ i^{-*}_{\beta u} = -2\dfrac{P^{-*}_{\alpha u}v^+_{\beta s} + P^{-*}_{\beta u}v^+_{\alpha s}}{V^{+2}} \\ V^{+2} = v^{+2}_{\alpha s} + v^{+2}_{\beta s}. \end{cases} \tag{28}$$

Also, additional transformation is needed to convert these references into negative-sequence three-phase values. The transformation matrix T is represented as

$$T = \begin{bmatrix} 1 & 0 \\ -\dfrac{1}{2} & -\dfrac{\sqrt{3}}{2} \\ -\dfrac{1}{2} & \dfrac{\sqrt{3}}{2} \end{bmatrix}. \tag{29}$$

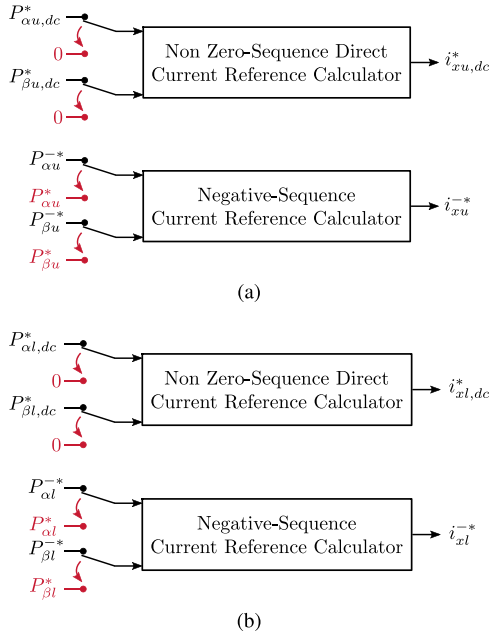

Fig. 10. Input modification of current reference calculators for the healthy pole after pole fault detection of the other pole. (a) In the case of negative-pole fault. (b) In the case of positive-pole fault.

The complete negative-sequence current reference calculators are depicted in Fig. 9(c). Note that due to the opposite sign of the inputs to the negative-sequence current reference calculators followed by (22)–(25), relationship between i^{-*}_{xu} and i^{-*}_{xl} can be deduced as

$$i^{-*}_{xu} = -i^{-*}_{xl}. \tag{30}$$

C. Comparison With Conventional MMC Control [12]

As upper and lower arm currents are controlled separately, the conventional circulating current injection for arm energy balancing is no more feasible since the injection relies on the symmetric operation of both upper and lower arms. Instead, the proposed control can naturally result in injection of circulating currents in an indirect manner, by controlling upper and lower arm currents with the derived references in (26) and (30) when both poles of the MMC are healthy. This sustains one of the most important advantages of the conventional MMC control: The energy balancing control is merely based on the circulating current injection inside the MMC and is fully independent and decoupled from the ac- and dc-side currents.

1) Total Energy: Total energy can be properly controlled as (8) and (10) are successfully regulated. The sum of ac grid active powers flowing through upper and lower arms contribute to the total energy control using commonly controlled q-axis currents of both arms.

2) Leg Energy: Each sum of leg energy can be managed to the same value if (9) and (11) are achieved. This can be done thanks to the power references derived from (18)-(21). It is important to note that since non zero-sequence current references have relationship as (26), they do not appear in both ac and dc sides like conventional circulating currents.

3) $\alpha\beta$ Arm Energy Difference: Each $\alpha\beta$ arm energy difference can also be controlled when (9) and (11) are achieved. The power references calculated in (22)-(25) deal with this energy difference control. Similar to the case of leg energy control, the negative-sequence currents of both arms act as negative-sequence circulating currents due to (30).

4) Zero-Sequence Arm Energy Difference: In [12], energy difference between the upper and lower arms, which commonly appears in every leg, is controlled by positive-sequence circulating current. Similarly, differences between the q-axis currents of both arms equally flow through every leg if the proposed control method is applied. In this way, the zero-sequence arm energy difference can be controlled to zero.

V. Proposed Fault-Tolerant Control

This section provides control strategies to deal with a single pole fault and unbalanced ac grid condition. Based on the aforementioned control scheme, these faulty conditions are handled by appropriately adjusting power references. Furthermore, an SLG ac FRT strategy is also integrated to validate the flexibility of the proposed control scheme.

A. Energy Balancing Control for Asymmetrical Monopole Operation Mode

If a permanent single pole fault is detected, the system configuration turns into the asymmetrical monopole configuration by blocking and disconnecting the faulty pole. As a consequence, circulating current injection through the MMC leg is no longer feasible circuit-wise. Instead, a negative-sequence phase current injection [7] is the feasible way as a compromise to balance the healthy arm energy since offset voltage cannot be injected due to the interconnection of zigzag transformer star point and dc-side neutral point.

And for seamless transition of energy balancing control mode, inputs to the current reference calculators can be simply modified as shown in Fig. 10, when the other pole fault is detected. In consequence, the non zero-sequence direct current references are changed to zero in the asymmetrical monopole operation mode. Therefore, continuous energy balancing in the healthy pole is ensured using the negative-sequence currents injected into the ac side. As the upper and lower arm currents are controlled separately, the current controller of the healthy pole operates seamlessly and tracks modified current references rapidly while the other controller is disabled.

B. Feedforward Control Strategy Under Unbalanced AC Grid Conditions

Considering imbalances and asymmetrical faults on the ac grid which are likely to occur in distribution systems, energy balancing control should be modified to improve the dynamic control performance [10], [27]. Feedforward terms are utilized in the proposed control scheme, but in a slightly different manner compared to the existing MMC control schemes, in order to preserve the independence between both poles.

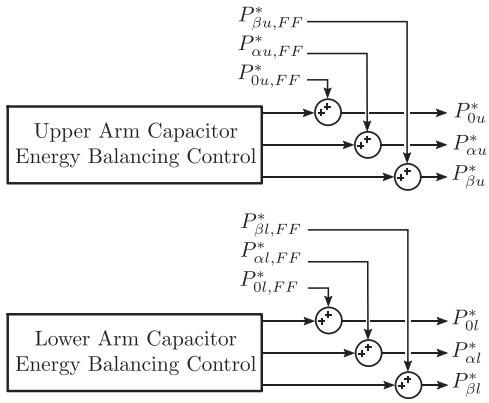

Fig. 11. Modified energy balancing controllers including feedforward terms.

Since negative-sequence phase voltages are not negligible under unbalanced ac grid conditions, aforementioned energy balancing controllers, which are designed for normal operation, have to deal with large disturbances. In order to cancel these disturbances, the following feedforward terms are compensated to energy balancing controllers of both poles:

$$\begin{cases} P_{0u,FF} = \dfrac{v^-_{\alpha s} i^{-*}_{\alpha u} + v^-_{\beta s} i^{-*}_{\beta u}}{2} \\ P_{\alpha u,FF} = \dfrac{v^-_{\alpha s} i^{+*}_{\alpha u} - v^-_{\beta s} i^{+*}_{\beta u}}{2} \\ P_{\beta u,FF} = -\dfrac{v^-_{\alpha s} i^{+*}_{\beta u} + v^-_{\beta s} i^{+*}_{\alpha u}}{2} \end{cases} \tag{31}$$

$$\begin{cases} P_{0l,FF} = \dfrac{v^-_{\alpha s} i^{-*}_{\alpha l} + v^-_{\beta s} i^{-*}_{\beta l}}{2} \\ P_{\alpha l,FF} = \dfrac{v^-_{\alpha s} i^{+*}_{\alpha l} - v^-_{\beta s} i^{+*}_{\beta l}}{2} \\ P_{\beta l,FF} = -\dfrac{v^-_{\alpha s} i^{+*}_{\beta l} + v^-_{\beta s} i^{+*}_{\alpha l}}{2}. \end{cases} \tag{32}$$

A detailed derivation process of these terms is given in the Appendix. Note that it is reasonable to use each pole current references for the calculation because of relatively low energy balancing control bandwidth compare to current control bandwidth [28]. The modified energy balancing controllers including feedforward terms are depicted in Fig. 11.

C. AC SLG FRT Strategy Integration

Integration of ac SLG FRT strategy is needed to deal with modern grid codes which require continuous stable operation of converter under asymmetrical ac side faults. Although various ac SLG FRT strategies for MMC stations have been proposed [29], an FRT scheme proposed in [27] is chosen as an example and is extended to the zigzag MMC to demonstrate the flexibility of the proposed independent pole control scheme in this article.

FRT controllers during an SLG fault on the rectifier-mode MMC are established for both poles as shown in Fig. 12. Pole voltages are varied by the rectifier-mode MMC to inform the inverter-mode MMC that there is a lack of instantaneous active-power capacity due to the ac grid voltage sag. The differences

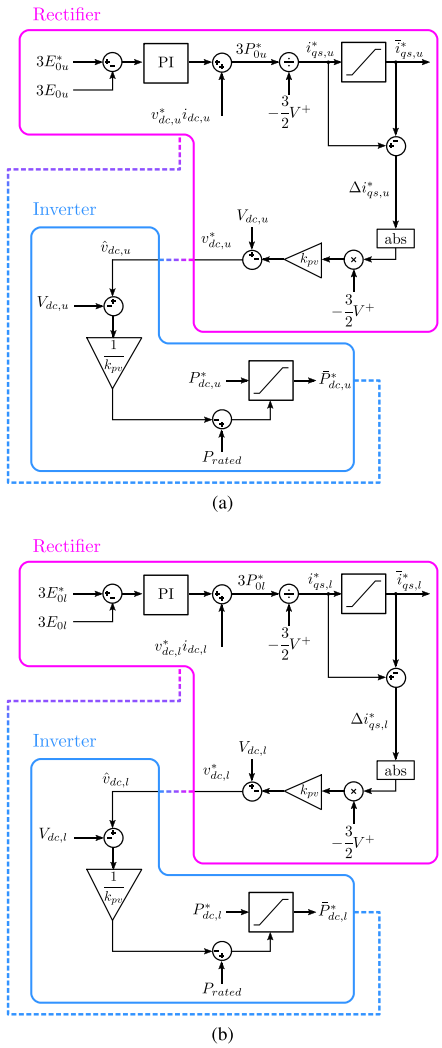

Fig. 12. Integration of the AC SLG FRT controllers into the proposed control scheme. (a) Positive pole. (b) Negative pole.

between the q-axis current references before and after the saturation block is used to modify the pole voltage references of the rectifier-mode MMC. By estimating pole voltage references considering voltage drop by cable resistance, the inverter-mode MMC immediately limits the dc-side power references based on the predetermined pole voltage and power reference slope.

Furthermore, the power flow controller for the inverter-mode MMC is also duplicated to handle the active power flow of each pole, as shown in Fig. 13. Since pole currents are used to regulate dc-side power flow, saturation blocks are first applied to power references considering the ac grid voltage sag and then both pole current references are derived. With these power flow controllers, FRT during an SLG fault on the inverter-mode MMC can be valid for both poles.

VI. Controller Hardware-in-The-Loop Validation

To verify the proposed independent pole control scheme using a controller hardware in real time, a CHIL test system is configured as shown in Fig. 14. An OPAL-RT real-time

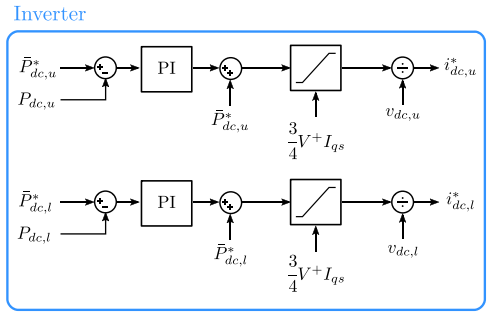

Fig. 13. Duplicated power flow controllers of the inverter-mode MMC. (I_{qs} denotes the rated q-axis current of MMC.)

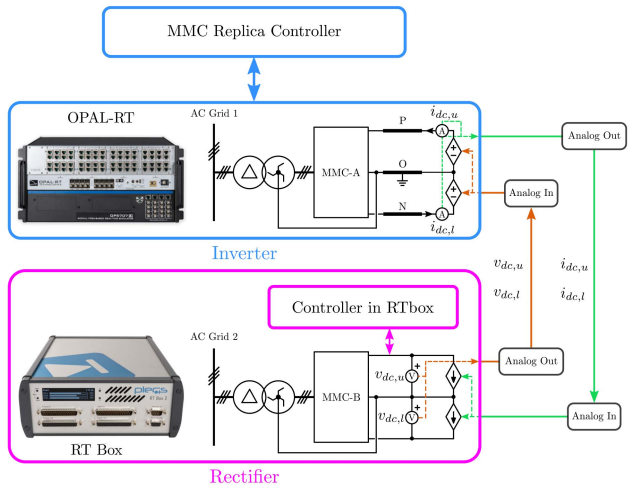

Fig. 14. System configuration used in the CHIL test.

simulator emulates distribution cables and a single zigzag MMC, referred to as MMC-A. MMC-A connected to ac grid 1 operates in the inverter mode where the active power of each pole is controlled with the pole current reference of each corresponding pole. An RT Box also emulates the other zigzag MMC, referred to as MMC-B. MMC-B connected to ac grid 2 operates in the rectifier mode which maintains the dc voltages of both poles at the rated pole voltage. All submodules of the zigzag MMC are configured using half-bridge submodules. In addition, an ideal transformer model is used to link both poles in the real-time simulator, enabling the configuration of a point-to-point MVDC distribution system. Measured pole voltages and currents are exchanged via analog input and output channels of real-time simulators, and then the measured values are realized with controllable voltage and current sources. Note that the neutral points of the MVDC cables, namely the dedicated metallic return conductors, are solidly grounded.

The whole CHIL test setup is shown in Fig. 15. A dedicated MMC replica controller is connected to the OPAL-RT real-time simulator, and the proposed control scheme for the inverter-mode station is implemented on the replica controller forming a CHIL test environment. On the other hand, the proposed control scheme for the rectifier-mode station is implemented on the RT Box using rapid control prototyping functionality,

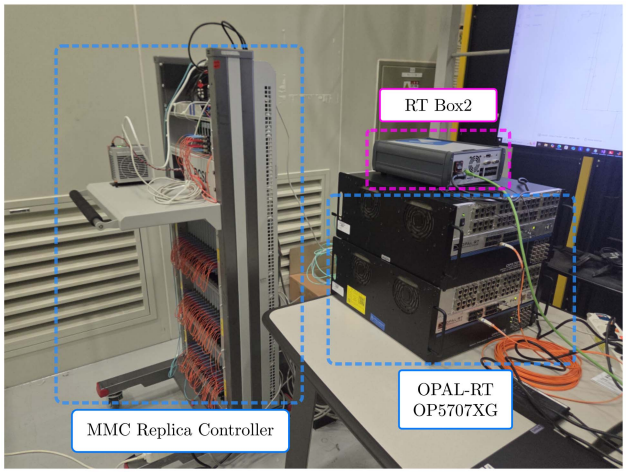

Fig. 15. Implemented CHIL test setup.

TABLE III
PARAMETERS USED IN THE CHIL TEST SYSTEM

MMC	
Rated power	10 MW
Rated pole voltage	±10 kV
Rated pole current	500 A
Submodules per arm	8
Submodule capacitor voltage	2.5 kV
Submodule capacitance	2.7 mF
Arm inductance	5.8 mH (18%)
Sampling frequency	5 kHz
Zigzag Transformer	
Primary-side voltage	22.9 kV
Secondary-side voltage	11 kV
Rated apparent power	11 MVA
Leakage percent impedance	5%
MVDC Cable	
Cable resistance	0.07 Ω/km
Cable inductance	0.35 mH/km
Cable length	20 km
Real-time Simulator	
Time step of the RT Box	5 μs
Time step of the OPAL-RT simulator	2 μs

which emulates a controller and system model simultaneously. The detailed parameters of the CHIL test system are listed in Table III.

A. Normal Operation

First, in order to validate the proposed MMC control scheme for bipole operation, simulation under normal condition is conducted and the results are shown in Fig. 16. Since the startup sequence of both converter stations is not the main focus of this article, the initial operation phases of both converters are excluded. At $t = 0$s, the positive pole of MMC-A starts to draw active power from 0 p.u. to 1 p.u. by controlling the positive-pole current while the negative pole of MMC-A keeps idle operation. At the same time, the positive pole of MMC-B supplies active power from the ac side to the dc side accordingly. As a result, as shown in Fig. 16, only the upper arm currents mainly conduct while the lower arm currents are nearly controlled to zero. The averaged submodule capacitor voltages of both poles are also successfully controlled to the rated voltage while both sides are controlled separately.

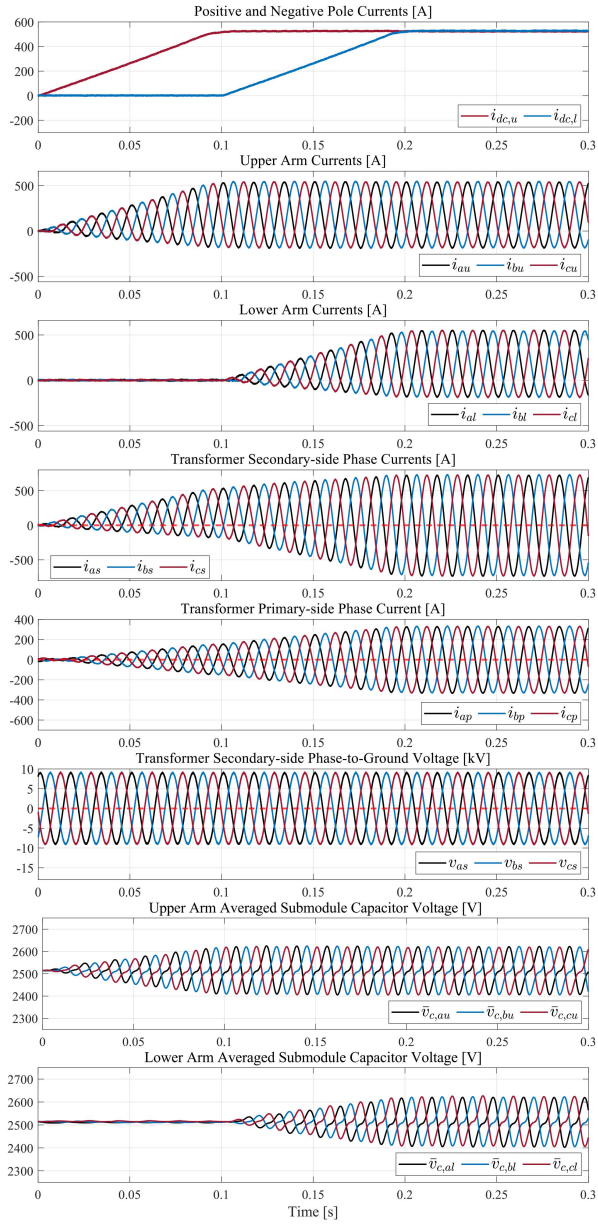

Fig. 16. CHIL test results of MMC-A operating in normal condition. (The red dashed line indicates the zero value.)

It is important to note that the secondary-side currents of the transformer have significant dc offsets when the active powers of both poles are unbalanced. However, these offsets can be

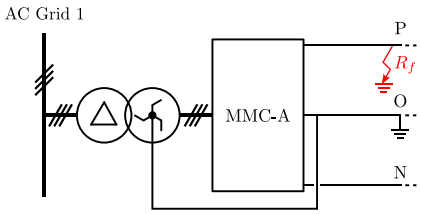

Fig. 17. Positive PtG fault scenario at the MMC-A side.

endured without core saturation by adopting the zigzag winding which cancels out zero-sequence flux. Furthermore, it can be observed that the primary-side currents and the secondary-side phase-to-ground voltages do not contain any zero-sequence dc offsets, which also reflects the unique feature of the zigzag transformer.

At $t = 0.1$ s, the negative pole of MMC-A independently draws active power from 0 p.u. to 1 p.u. while the positive pole of MMC-A continues to operate at its rated condition. Finally, as shown in Fig. 16, both poles of MMC-A draw equal active power simultaneously, maintaining the balanced submodule capacitor voltages.

These results confirm that the bipole operation of both poles under normal conditions can be also achieved using the proposed control scheme.

B. Operation Under Pole-to-Ground Fault

To verify the effectiveness of the proposed control scheme under a single pole fault, a scenario which contains a positive PtG fault at the MMC-A side is tested as shown in Fig. 17. In this scenario, the ground fault resistance is set to 1 Ω.

As shown in Fig. 18, both poles of MMC-A initially draw 1 p.u. active power from dc side, while MMC-B operates accordingly in pre-fault phase. At $t = 20$ ms, a positive PtG fault occurs at the MMC-A side and large fault currents flow through the star point of the transformer secondary side. Following a fault clearing sequence in response, the upper arm submodules are turned into blocking mode and DCCB isolates the faulty pole within 2 ms. For the sake of simplicity, it is assumed that both converters detect the fault simultaneously and the time required for the protection is the same.

Meanwhile, the negative poles of both converters operate in the pre-fault rated condition regardless of PtG fault occurring at the other pole. Since the proposed control strategy separates the control of each pole, the lower arm currents can be continuously controlled to the desired value. Although the lower arm currents are slightly distorted before fault clearance, this does not seriously affect the healthy pole operation during the short-circuit fault event. Therefore, the dc-side power delivery of the negative pole can be sustained without an interruption.

In addition, the upper arm averaged capacitor voltages of MMC-A remain unchanged after entering blocking mode as shown in Fig. 18. On the other hand, the lower arm averaged capacitor voltages of MMC-A are nicely balanced in the rated voltage within the whole time region. This is because the proposed energy-balancing mode transition scheme is seamlessly

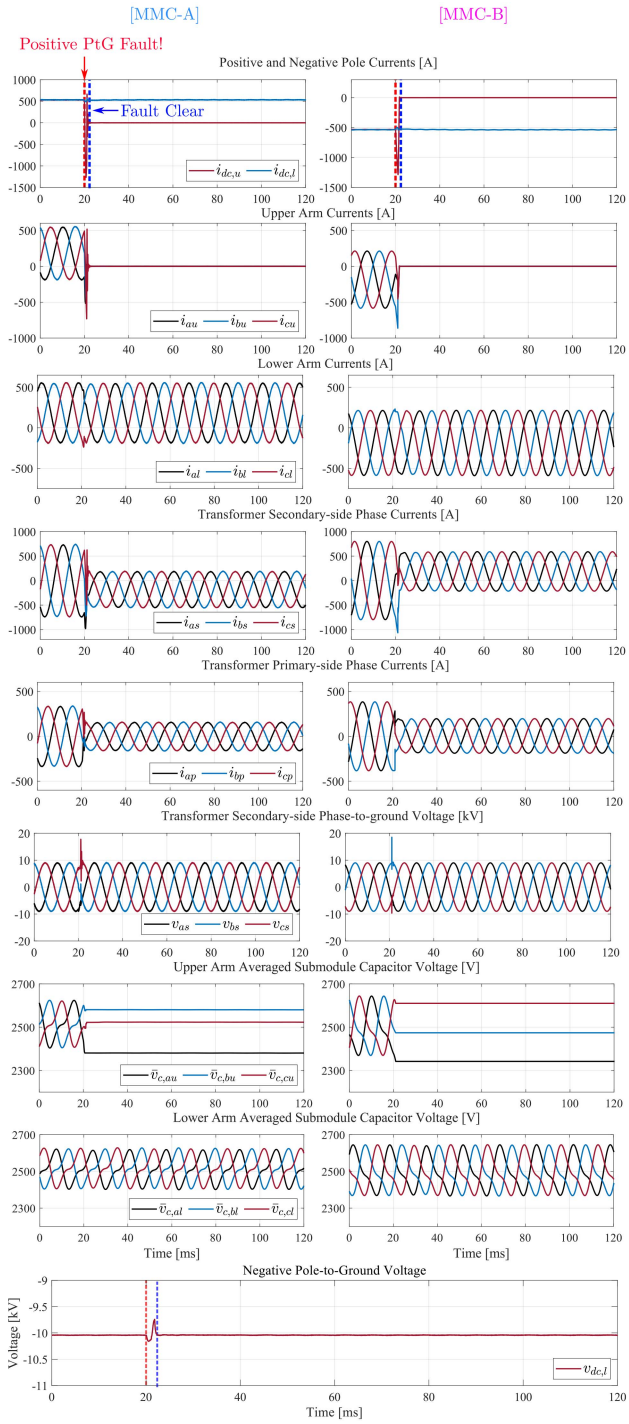

Fig. 18. CHIL test results under the positive PtG fault condition. (DCCB clears the fault.)

applied after the fault detection so that the negative-sequence phase currents are injected to the ac grid temporarily for the healthy pole energy balancing.

Furthermore, another CHIL test is performed to validate both the fault clearing strategy using ACCB and the proposed control scheme. As shown in Fig. 19, the same positive PtG fault scenario is applied at $t = 20$ ms and the positive pole of

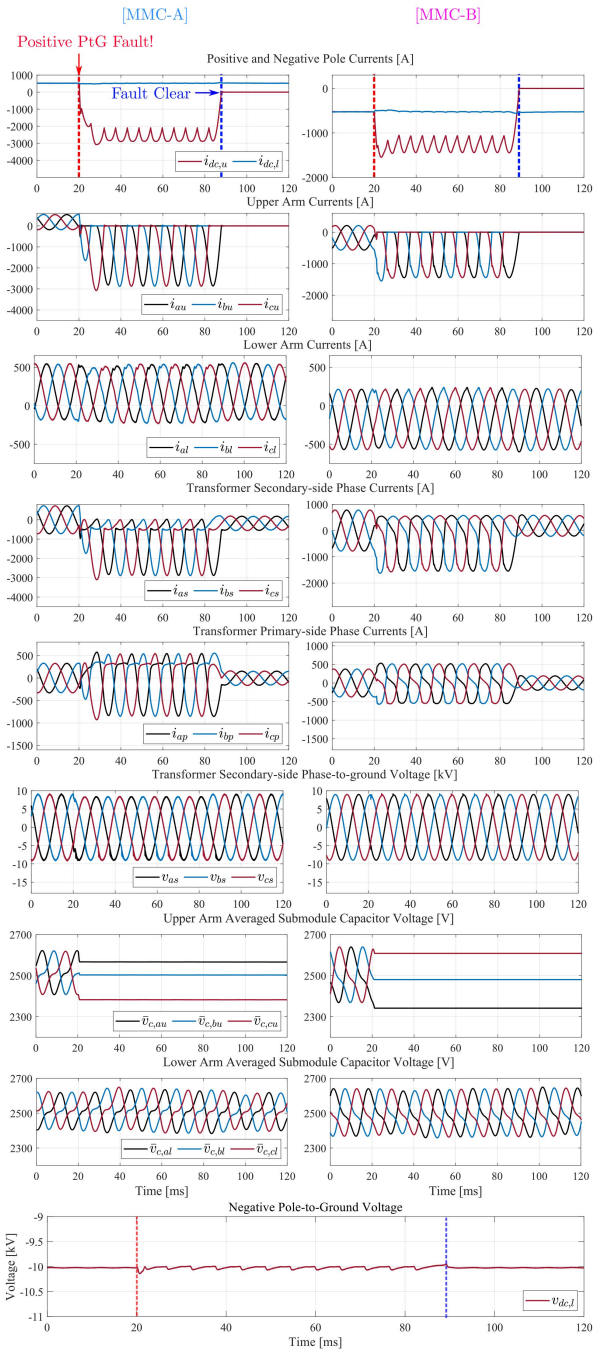

Fig. 19. CHIL test results under the positive PtG fault condition. (ACCB clears the fault.)

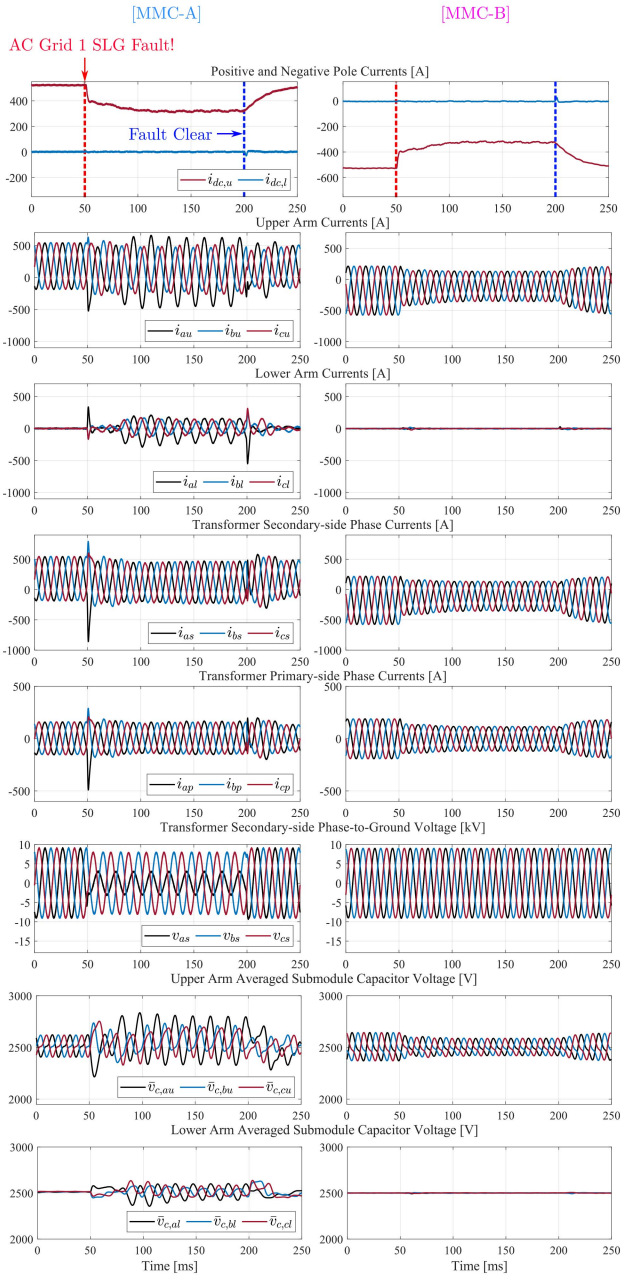

Fig. 20. CHIL test results under SLG fault condition on AC grid 1.

MMC-A is blocked sequentially. Within approximately 60 ms, the ACCB in the upper arm clears the fault by operating at the natural zero-crossing point of the arm current. Similarly, the negative pole continues to operate in the rated condition after the fault clearance. Although significant fault currents occur in the positive pole, the submodules are protected by protection bypass thyristors, and the passive components, such as transformer windings and arm reactors, are practically designed to withstand these transient fault currents in accordance with the overall protection coordination scheme [20], [21]. Consequently, the overall system remains undamaged under such fault conditions.

These results demonstrate the validity of the proposed control scheme, which preserves the independence of both poles even if a single pole undergoes severe PtG fault.

C. AC SLG FRT

Operation under the ac SLG fault conditions are tested to validate the integrated ac SLG FRT strategy. Since the ac SLG FRT strategy is separately integrated to each pole, initial operating points of both poles are intentionally set to different values. Consequently, it is assumed that the positive pole of

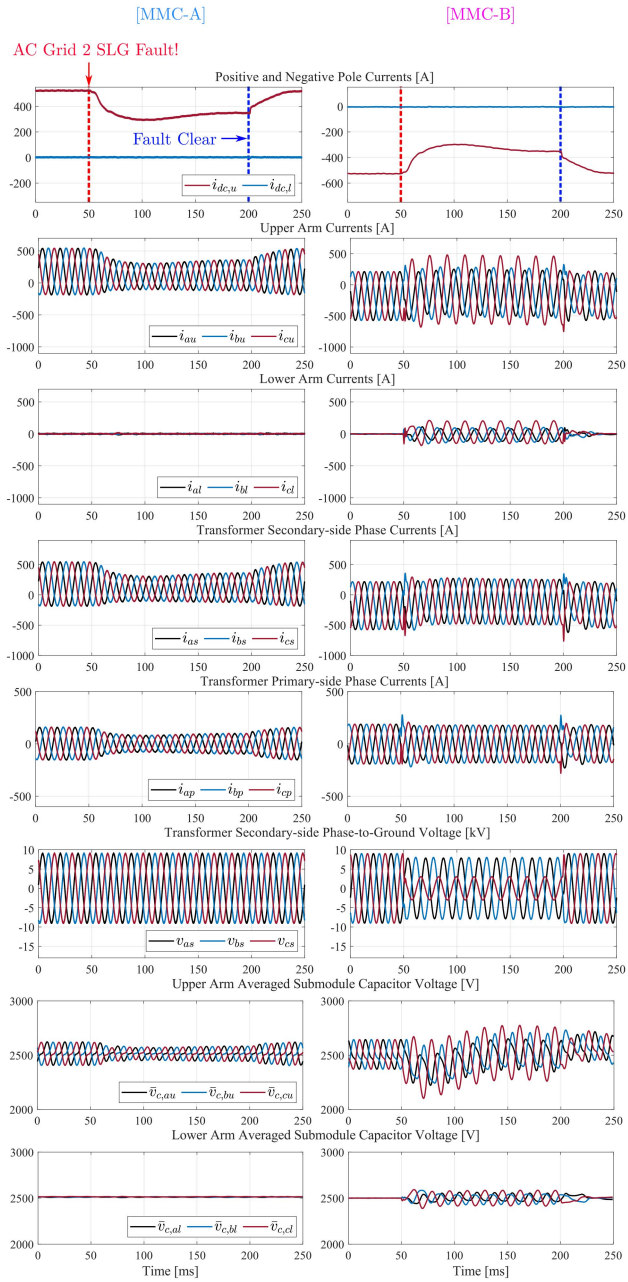

Fig. 21. CHIL test results under SLG fault condition on AC grid 2.

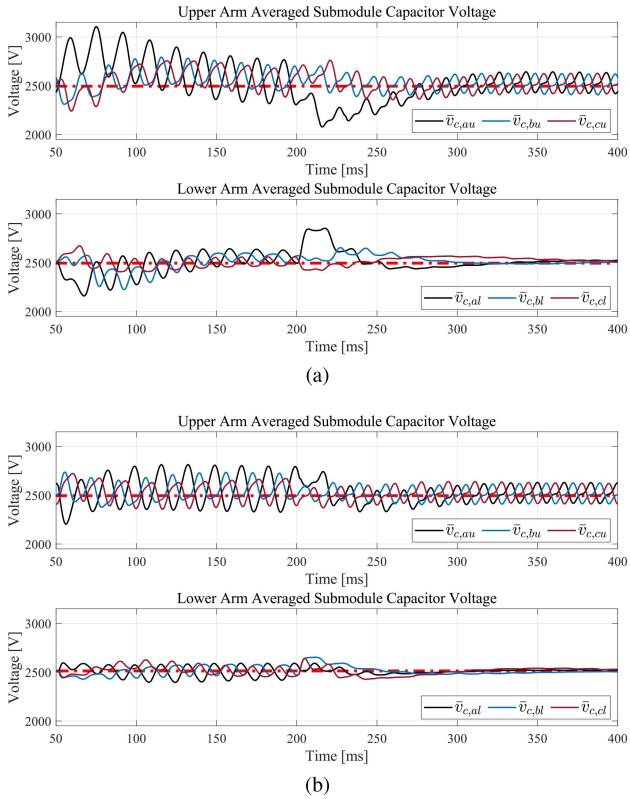

Fig. 22. Comparison of the averaged submodule capacitor voltages of MMC-A with and without feedforward terms under unbalanced AC grid conditions. (The red dash-dot pattern denotes the nominal value of the submodule capacitor voltage.) (a) Test results when the feedforward terms are not applied. (b) Test results when the feedforward terms are applied.

TABLE IV
PARAMETERS OF THE DOWNSCALED EXPERIMENTAL SETUP

MMC	
Rated power	4 kW
Rated pole voltage	±180 V
Rated pole current	11 A
Submodules per arm	6
Submodule capacitor voltage	60 V
Submodule capacitance	2.39 mF
Arm inductance	4 mH (14%)
Sampling frequency	10 kHz
Zigzag Transformer	
Primary-side voltage	133 V
Secondary-side voltage	200 V

MMC-A draws 1 p.u. active power from the dc side while the negative pole keeps idle operation with zero active power transfer.

As shown in Fig. 20, an SLG fault occurs in ac grid 1 at $t =$ 50 ms and the instantaneous power capacity of the positive pole is reduced to two-thirds of the rated pole power due to the ac grid voltage sag. The power flow controller reduces the positive-pole current references in response while the negative-pole current reference remains zero. Although upper arm currents increase to maintain the balance of the upper arm energies, the peak of the currents is within the stable range considering the submodule design margin. One may argue that lower arm currents simultaneously increase, even though there is no active power flow at the negative pole. This results from the power reference coupling between the upper and lower arms, which leads to the indirect injection of circulating currents to maintain energy balance across all arms as in [27]. At $t = 200$ ms, the fault is cleared 150 ms later and the positive pole returns to the initial operation point.

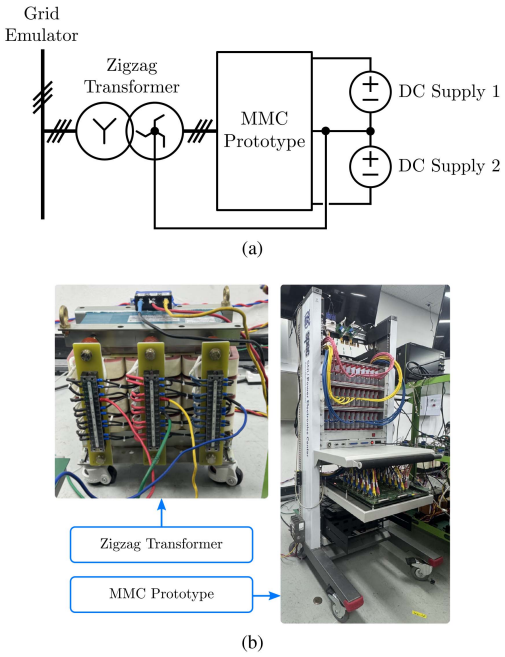

Fig. 23. Implemented downscaled experimental setup. (a) Schematic diagram of the experimental setup. (b) Photograph of the experimental setup.

As shown in Fig. 21, an SLG fault is applied in ac grid 2 at $t = 50$ ms to evaluate the coordination between the power flow controller and the FRT controller, implemented in MMC-A and MMC-B, respectively. The FRT controller adjusts the positive-pole voltage reference of MMC-B to inform MMC-A that there is a lack of power capacity at the positive pole. In consequence, the power flow controller limits the positive-pole current reference so that the upper arm currents are reduced in response. Same as the previous SLG fault, the fault is cleared after 150 ms. Notably, the averaged submodule capacitor voltages are consistently well balanced over the entire time interval.

Furthermore, an additional test is conducted without employing the feedforward terms under unbalanced ac grid conditions. The effect of the feedforward terms on energy balancing control performance is then investigated by comparing the averaged submodule capacitor voltages, as shown in Fig. 22. As shown in Fig. 22(a), the averaged submodule capacitor voltages initially diverge and it takes certain time to converge to the nominal value when the feedforward terms are not applied. In contrast, the energy balancing control utilizing the feedforward terms quickly addresses disturbances under the ac grid voltage sag, enabling rapid convergence of the averaged submodule capacitor voltages as shown in Fig. 22(b).

The test results show that the proposed control scheme not only ensures the independent pole operation capability, but also enables independent response under unbalanced conditions including SLG faults.

VII. Experimental Results

Several experiments are conducted with a downscaled MMC prototype to validate the performance of the proposed independent pole control scheme. An experimental setup is configured as depicted in Fig. 23(a), which consists of a grid emulator, a zigzag transformer, a single MMC prototype, and two dc power supplies. As shown in Fig. 23(b), the zigzag transformer is implemented with a multiwinding transformer, which consists of wye windings on the primary side and multiple open windings on the secondary side. In addition, as dc power supplies maintain pole voltages, the proposed control scheme for the inverter-mode station is implemented on the controller. The detailed parameters of the experimental setup are listed in Table IV.

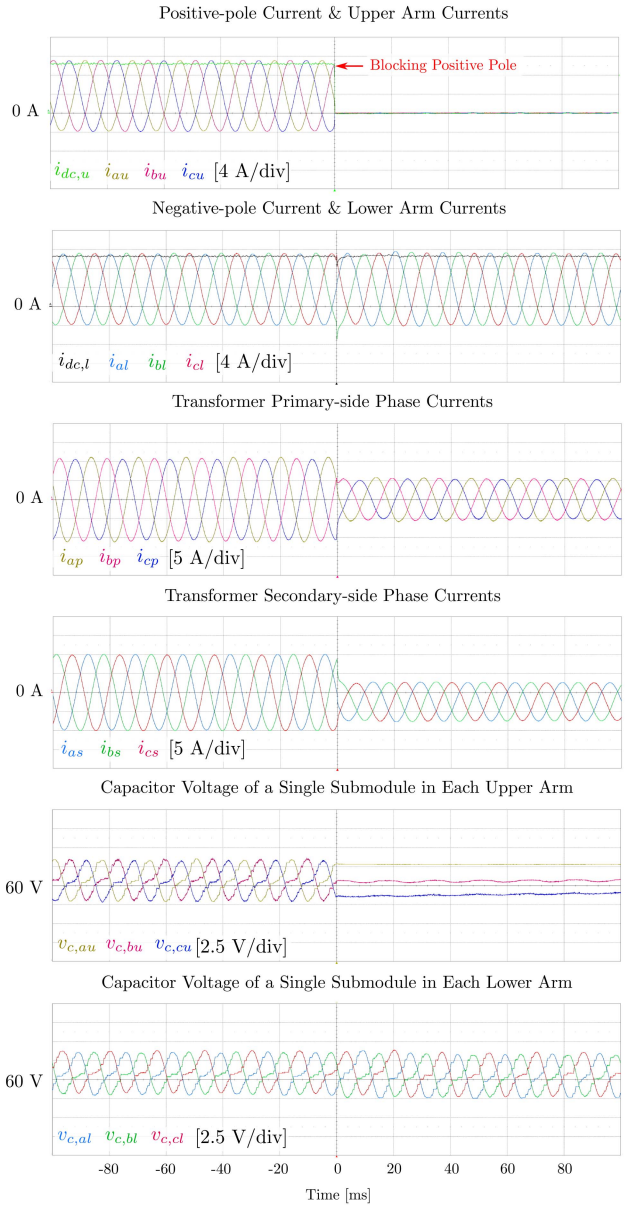

Fig. 24. Experimental results with the proposed control scheme when the positive pole turns into the blocking mode abruptly.

A. Single-Pole Blocking

As submodules in the MMC prototype are not equipped with the protection bypass thyristors, experiment under PtG fault

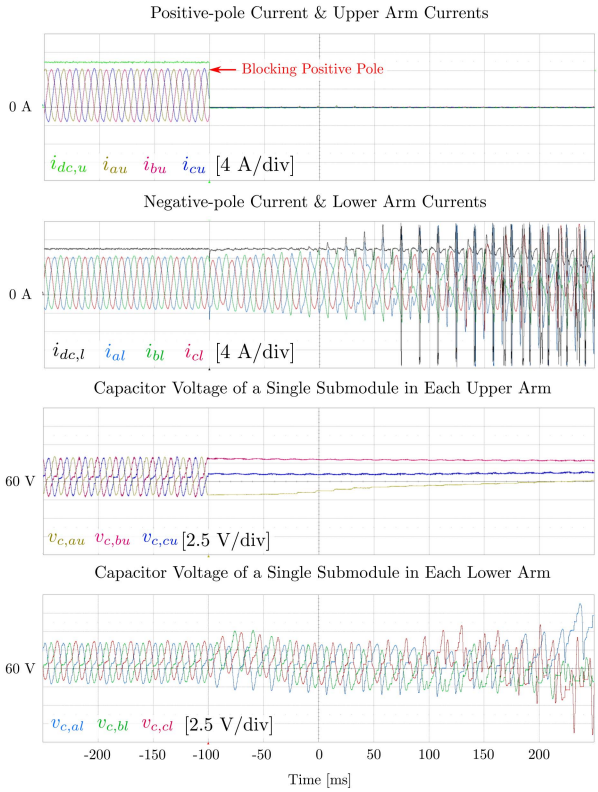

Fig. 25. Experimental results with the control scheme in [6] when the positive pole turns into the blocking mode abruptly.

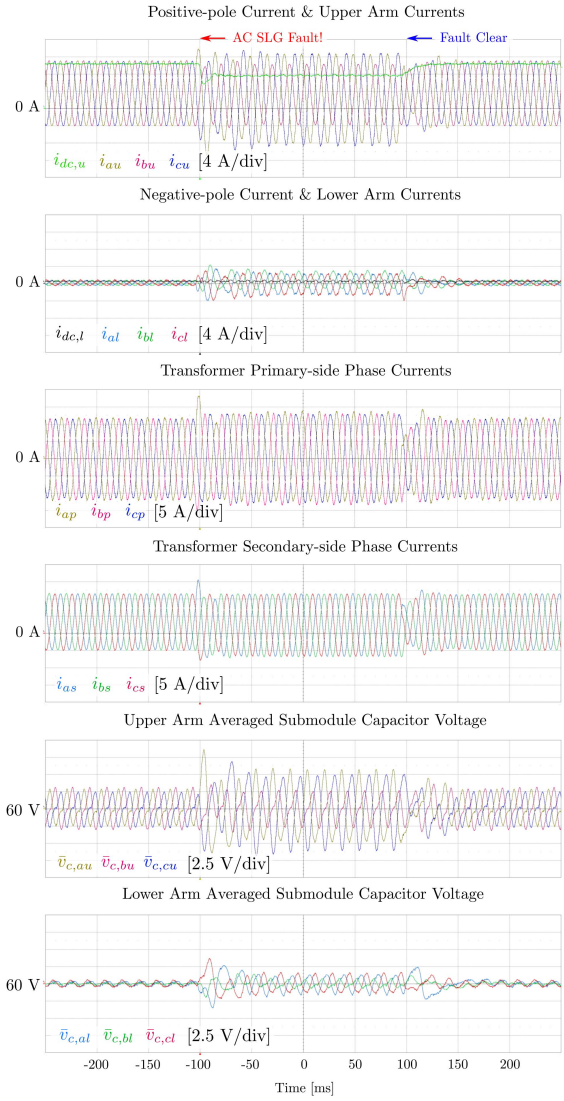

Fig. 26. Experimental results under SLG fault condition.

scenario is impossible to be conducted unlike the CHIL test. Instead, an abrupt transition to the blocking mode on a single pole is performed while both poles are delivering the rated active power to the ac grid to emulate the postfault scenario after a PtG fault. This action represents a severe operating condition to validate the transient performance of the proposed control scheme.

Before $t = 0$ ms, both poles draw 1 p.u. active power from dc power supplies by controlling pole currents, as shown in Fig. 24. At $t = 0$ ms, the positive pole turns into the blocking mode within 100 μs, causing the arm currents to rapidly shrink to zero. In consequence, it can also be observed that capacitor voltages of submodules in the positive pole remain nearly constant. On the other hand, the negative pole continues to operate under the rated active power condition, even when the other pole has stopped operation. At the same time, energy balancing control seamlessly turns into the asymmetrical monopole operation mode ensuring that the capacitor voltages of submodules in the negative pole remain continuously balanced at their nominal values.

Furthermore, an additional experiment is conducted using the control and mode transition scheme in [6], which relies on the conventional MMC modeling and dependent control of both poles. While both poles identically draw 1 p.u. active power, the positive pole turns into the blocking mode at $t = -100$ ms, which is shown in Fig. 25. Although the positive pole current and upper arm currents diminish to zero, the negative pole becomes unstable, exhibiting large fluctuations in both the arm currents and the capacitor voltages. Consequently, the negative pole cannot maintain continuous operation with the control scheme in [6].

These experimental results demonstrate that the proposed control scheme enables each pole to be operated independently with the seamless transition of the energy balancing control, even if a single pole becomes uncontrollable and ceases its operation.

B. AC SLG FRT

Similar to the CHIL test scenario, another experiment is conducted in which the positive pole initially draws 1 p.u. active power from dc supply 1, while the negative pole maintains a minimum active power transfer to maintain sorting and balancing of the submodule capacitor voltages within the same arm.

As shown in Fig. 26, the grid emulator then initiates the SLG fault at $t = -100$ ms, and the power flow controller

reduces the positive-pole current references in response while the negative-pole current reference remains unchanged. The arm currents of both poles increase to balance arm energies, which is consistent with the CHIL test result of MMC-A shown in Fig. 20. Although the primary-side currents of the transformer seems slightly unbalanced, this is mainly due to the nonlinear and significantly unbalanced three-phase magnetizing currents of the transformer induced by the abrupt change of the grid voltage as figured out in [30]. In contrast, the secondary-side currents of the transformer are well balanced by closed-loop current control and fully exploiting circulating currents through the power reference coupling proposed in this article. At $t =$ 100 ms, the fault is cleared and the positive pole restores its operation to the rated active power condition. Throughout the entire time interval including the SLG fault condition, the averaged submodule capacitor voltages are effectively kept balanced with the proposed control scheme.

These experimental results confirm the performance of the proposed control scheme and the integrated FRT strategy under SLG fault conditions.

VIII. Conclusion

This article presented the fault-tolerant independent pole control scheme of the zigzag MMC for bipolar MVDC distribution systems. The proposed control scheme addressed the challenge of maintaining independent control of each pole in the event of a fault in the other. Even though the arm current controllers and energy balancing controllers are separated within upper and lower arms, the benefit of conventional MMC circulating current based balancing control in the normal MMC can still be fully exploited and preserved through power reference coupling when both poles are healthy. When a severe single pole fault such as a PtG fault occurs, this coupling can be seamlessly disabled by modifying the inputs of the current reference calculators, thereby ensuring continuous energy balancing in the healthy pole. Furthermore, the existing ac SLG FRT strategy was integrated into the proposed control scheme, incorporating feedforward terms and additional controllers to preserve the independence of both poles. The effectiveness of the proposed control strategy was validated through the CHIL test, demonstrating the control performance under both single PtG fault and ac SLG fault scenarios. Finally, experiments conducted with a downscaled MMC prototype and a zigzag transformer validated the performance of the proposed control scheme under abrupt single-pole blocking and ac SLG fault conditions.

Appendix

Firstly, generic positive-sequence phase voltages and currents of upper arm can be represented as

$$\begin{cases} v_{as}^{+} = V^{+}\cos(\omega t) \\ v_{bs}^{+} = V^{+}\cos(\omega t - \dfrac{2\pi}{3}) \\ v_{cs}^{+} = V^{+}\cos(\omega t + \dfrac{2\pi}{3}) \end{cases} \tag{33}$$

$$\begin{cases} i_{au}^{+} = I^{+}\cos(\omega t - \phi_i^{+}) \\ i_{bu}^{+} = I^{+}\cos(\omega t - \phi_i^{+} - \dfrac{2\pi}{3}) \\ i_{cu}^{+} = I^{+}\cos(\omega t - \phi_i^{+} + \dfrac{2\pi}{3}) \end{cases} \tag{34}$$

where ϕ_i^{+} denotes the phase difference between positive-sequence phase voltage and current.

In the case of negative-sequence phase voltages and currents of upper arm, they can be also represented as

$$\begin{cases} v_{as}^{-} = V^{-}\cos(\omega t - \phi_v^{-}) \\ v_{bs}^{-} = V^{-}\cos(\omega t - \phi_v^{-} + \dfrac{2\pi}{3}) \\ v_{cs}^{-} = V^{-}\cos(\omega t - \phi_v^{-} - \dfrac{2\pi}{3}) \end{cases} \tag{35}$$

$$\begin{cases} i_{au}^{-} = I^{-}\cos(\omega t - \phi_i^{-}) \\ i_{bu}^{-} = I^{-}\cos(\omega t - \phi_i^{-} + \dfrac{2\pi}{3}) \\ i_{cu}^{-} = I^{-}\cos(\omega t - \phi_i^{-} - \dfrac{2\pi}{3}) \end{cases} \tag{36}$$

where ϕ_v^{-} and ϕ_i^{-} denote the phase differences between positive-sequence phase voltage and negative-sequence phase voltage and current.

Second, averaged power disturbances in upper arm yielded by negative-sequence phase voltages can be deduced as follows:

$$\begin{cases} P_{au} = -\dfrac{V^{-}I^{+}}{2}\cos(\phi_i^{+} - \phi_v^{-}) - \dfrac{V^{-}I^{-}}{2}\cos(\phi_i^{-} - \phi_v^{-}) \\ P_{bu} = -\dfrac{V^{-}I^{+}}{2}\cos(\phi_i^{+} - \phi_v^{-} - \dfrac{2\pi}{3}) \\ \qquad -\dfrac{V^{-}I^{-}}{2}\cos(\phi_i^{-} - \phi_v^{-}) \\ P_{cu} = -\dfrac{V^{-}I^{+}}{2}\cos(\phi_i^{+} - \phi_v^{-} + \dfrac{2\pi}{3}) \\ \qquad -\dfrac{V^{-}I^{-}}{2}\cos(\phi_i^{-} - \phi_v^{-}). \end{cases} \tag{37}$$

After applying Clarke transformation, these power disturbances are represented as follows:

$$\begin{cases} P_{0u} = -\dfrac{V^{-}I^{-}}{2}\cos(\phi_i^{-} - \phi_v^{-}) \\ P_{\alpha u} = -\dfrac{V^{-}I^{+}}{2}\cos(\phi_i^{+} - \phi_v^{-}) \\ P_{\beta u} = -\dfrac{V^{-}I^{+}}{2}\sin(\phi_i^{+} - \phi_v^{-}). \end{cases} \tag{38}$$

Lastly, (34), (35), and (36) can also be Clarke transformed as follows:

$$\begin{cases} i_{\alpha u}^{+} = I^{+}\cos(\omega t - \phi_i^{+}) \\ i_{\beta u}^{+} = I^{+}\sin(\omega t - \phi_i^{+}) \end{cases} \tag{39}$$

$$\begin{cases} v_{\alpha s}^{-} = V^{-}\cos(\omega t - \phi_v^{-}) \\ v_{\beta s}^{-} = -V^{-}\sin(\omega t - \phi_v^{-}) \end{cases} \tag{40}$$

$$\begin{cases} i_{\alpha u}^{-} = I^{-}\cos(\omega t - \phi_i^{-}) \\ i_{\beta u}^{-} = -I^{-}\sin(\omega t - \phi_i^{-}). \end{cases} \tag{41}$$

Based on the trigonometric identities, below feedforward terms are derived using (38) and (39)–(41)

$$\begin{cases} P_{0u,FF} = -P_{0u} = \dfrac{v_{\alpha s}^{-} i_{\alpha u}^{-*} + v_{\beta s}^{-} i_{\beta u}^{-*}}{2} \\ P_{\alpha u,FF} = -P_{\alpha u} = \dfrac{v_{\alpha s}^{-} i_{\alpha u}^{+*} - v_{\beta s}^{-} i_{\beta u}^{+*}}{2} \\ P_{\beta u,FF} = -P_{\beta u} = -\dfrac{v_{\alpha s}^{-} i_{\beta u}^{+*} + v_{\beta s}^{-} i_{\alpha u}^{+*}}{2}. \end{cases} \tag{42}$$

For the lower arms, feedforward terms can be similarly derived by repeating the same procedure.

REFERENCES

[1] R. W. De Doncker, "Power electronic technologies for flexible DC distribution grids," in *Proc. Int. Power Electron. Conf. (IPEC-Hiroshima 2014 - ECCE ASIA)*, May 2014, pp. 736–743.

[2] S. Debnath, J. Qin, B. Bahrani, M. Saeedifard, and P. Barbosa, "Operation, control, and applications of the modular multilevel converter: A review," *IEEE Trans. Power Electron.*, vol. 30, no. 1, pp. 37–53, Jan. 2015.

[3] W. Leterme, P. Tielens, S. De Boeck, and D. Van Hertem, "Overview of grounding and configuration options for meshed HVDC grids," *IEEE Trans. Power Del.*, vol. 29, no. 6, pp. 2467–2475, Dec. 2014.

[4] T. Dragičević, X. Lu, J. C. Vasquez, and J. M. Guerrero,"DC Microgrids—Part II: A Review of Power Architectures, Applications, and Standardization Issues," *IEEE Trans. Power Electron.*, vol. 31, no. 5, pp. 3528–3549, May 2016.

[5] S. Cui, J.-H. Lee, J. Hu, R. W. De Doncker, and S.-K. Sul, "A modular multilevel converter with a zigzag transformer for bipolar MVDC distribution systems," *IEEE Trans. Power Electron.*, vol. 34, no. 2, pp. 1038–1043, Feb. 2019.

[6] S. Cui, J. Hu, and R. W. De Doncker, "Monopole operation of on-load faulty valves replacement of modular multilevel converters (MMCs) in bipolar MVDC grids," in *Proc. 2020 IEEE 9th Int. Power Electron. Motion Control Conf. (IPEMC2020-ECCE Asia)*, Jan. 2020, pp. 888–891.

[7] D. Soto-Sanchez and T. C. Green, "Control of a modular multilevel converter-based HVDC transmission system," in *Proc. 14th Eur. Conf. Power Electron. Appl.*, Aug. 2011, pp. 1–10.

[8] A. Junyent-Ferré, P. Clemow, M. M. Merlin, and T. C. Green, "Operation of HVDC modular multilevel converters under DC pole imbalances," in *Proc. 2014 16th Eur. Conf. Power Electron. Appl.*, Aug. 2014, pp. 1–10.

[9] W. Xiang, W. Lin, L. Xu, and J. Wen, "Enhanced independent pole control of hybrid MMC-HVDC system," *IEEE Trans. Power Del.*, vol. 33, no. 2, pp. 861–872, Apr. 2018.

[10] A. E. Leon and S. J. Amodeo, "Energy balancing improvement of modular multilevel converters under unbalanced grid conditions," IEEE Trans. Power Electron., vol. 32, no. 8, pp. 6628–6637, Aug. 2017.

[11] H. Wang, G. Tang, Z. He, and J. Yang, "Efficient grounding for modular multilevel HVDC converters (MMC) on the AC side," *IEEE Trans. Power Del.*, vol. 29, no. 3, pp. 1262–1272, Jun. 2014.

[12] S. Cui, S. Kim, J.-J. Jung, and S.-K. Sul, "A comprehensive cell capacitor energy control strategy of a modular multilevel converter (MMC) without a stiff DC bus voltage source," in *Proc. IEEE Appl. Power Electron. Conf. Expo. - APEC 2014*. Fort Worth, TX, USA: IEEE, Mar. 2014, pp. 602–609.

[13] J. Singh, S. Singh, and A. Singh, "Distribution transformer failure modes, effects and criticality analysis (FMECA)," *Eng. Failure Anal.*, vol. 99, pp. 180–191, May 2019.

[14] *IEEE Standard for Test Procedure for Thermal Evaluation of Insulation Systems for Liquid-Immersed Distribution, Power, and Regulating Transformers* IEEE Std C57.100-2022 (Revision of IEEE Std C57.100-2011), pp. 1–64, Mar. 2023.

[15] J. Hu, K. Xu, L. Lin, and R. Zeng, "Analysis and enhanced control of hybrid-MMC-based HVDC systems during asymmetrical DC voltage faults," *IEEE Trans. Power Del.*, vol. 32, no. 3, pp. 1394–1403, Jun. 2017.

[16] J.-J. Jung, S. Cui, J.-H. Lee, and S.-K. Sul, "A new topology of multilevel VSC converter for a hybrid HVDC transmission system," *IEEE Trans. Power Electron.*, vol. 32, no. 6, pp. 4199–4209, Jun. 2017.

[17] G. Abeynayake, G. Li, T. Joseph, J. Liang, and W. Ming, "Reliability and cost-oriented analysis, comparison and selection of multi-level MVDC converters," *IEEE Trans. Power Del.*, vol. 36, no. 6, pp. 3945–3955, Dec. 2021.

[18] X. Pei, O. Cwikowski, D. S. Vilchis-Rodriguez, M. Barnes, A. C. Smith, and R. Shuttleworth, "A review of technologies for MVDC circuit breakers," in *Proc. IECON 2016-42nd Annu. Conf. IEEE Ind. Electron. Soc.*, Oct. 2016, pp. 3799–3805.

[19] K. Friedrich, "Modern HVDC PLUS application of VSC in modular multilevel converter topology," in *Proc. IEEE Int. Symp. Ind. Electron.*, Jul. 2010, pp. 3807–3810.

[20] G. Tang, Z. Xu, and Y. Zhou, "Impacts of three MMC-HVDC configurations on AC system stability under DC line faults," *IEEE Trans. Power Syst.*, vol. 29, no. 6, pp. 3030–3040, Nov. 2014.

[21] M. Davies, M. Dommaschk, J. Dorn, J. Lang, D. Retzmann, and D. Soerangr, "HVDC plus—Basics and principle of operation," *Siemens AG*, Energy Sector, Germany, Technical Article, 2009.

[22] P. Münch, D. Görges, M. Izák, and S. Liu, "Integrated current control, energy control and energy balancing of modular multilevel converters," in *Proc. IECON 2010-36th Annu. Conf. IEEE Ind. Electron. Soc.*, Jan. 2010, pp. 150–155.

[23] S. Milovanović and D. Dujić, "Comprehensive comparison of modular multilevel converter internal energy balancing methods," *IEEE Trans. Power Electron.*, vol. 36, no. 8, pp. 8962–8977, Aug. 2021.

[24] P. Rodríguez, R. Teodorescu, I. Candela, A. V. Timbus, M. Liserre, and F. Blaabjerg, "New positive-sequence voltage detector for grid synchronization of power converters under faulty grid conditions," in *Proc. 2006 37th IEEE Power Electron. Specialists Conf.*, Jun. 2006, pp. 1–7.

[25] D. Kim, S.-K. Sul, and S. Cui, "Indirect-modulated MMC current control with voltage disturbance estimation and compensation," in *Proc. IEEE 10th Int. Power Electron. Motion Control Conf. (IPEMC2024-ECCE Asia)*, May 2024, pp. 2609–2613.

[26] L. Harnefors, A. Antonopoulos, S. Norrga, L. Angquist, and H.-P. Nee, "Dynamic analysis of modular multilevel converters," *IEEE Trans. Ind. Electron.*, vol. 60, no. 7, pp. 2526–2537, Jul. 2013.

[27] S. Cui, H.-J. Lee, J.-J. Jung, Y. Lee, and S.-K. Sul, "A comprehensive AC-Side single-line-to-ground fault ride through strategy of an MMC-Based HVDC system," *IEEE Trans. Emerg. Sel. Topics Power Electron.*, vol. 6, no. 3, pp. 1021–1031, Sep. 2018.

[28] S. Fan, K. Zhang, J. Xiong, and Y. Xue, "An improved control system for modular multilevel converters with new modulation strategy and voltage balancing control," *IEEE Trans. Power Electron.*, vol. 30, no. 1, pp. 358–371, Jan. 2015.

[29] S. D. Tavakoli, E. Prieto-Araujo, and O. Gomis-Bellmunt, "AC fault ride through in MMC-based HVDC systems," *IEEE Trans. Power Del.*, vol. 37, no. 4, pp. 2775–2786, Aug. 2022.

[30] H. Xie, L. Angquist, and H.-P. Nee, "Comparison of voltage and flux modulation schemes of STATCOMs regarding transformer saturation during fault recovery," *IEEE Trans. Power Syst.*, vol. 23, no. 4, pp. 1653–1661, Nov. 2008.

Dong-Joon Kim (Graduate Student Member, IEEE) received the B.S. degree in electrical and computer engineering, from Seoul National University, Seoul, South Korea, in 2021, where he is currently working toward the Ph.D. degree in electrical engineering.

His research interests include modular multilevel converter (MMC), hardware-in-the-loop simulation (HILS), and interaction of power systems and power converters.

Jaeyeon Park (Graduate Student Member, IEEE) received the B.S. and M.S. degrees in electrical engineering and computer science, from Seoul National University, Seoul, South Korea, in 2021 and 2023, respectively, where he is currently working toward the Ph.D. degree in electrical engineering.

His research interests include control and modeling of power electronics, control and power hardware-in-the-loops, and high-power motor drives for shipboard propulsion systems.

Yeonjoo Hong (Member, IEEE) received the B.S. degree in electrical and electronic engineering from Konkuk University, Seoul, Korea, in 2019, and the M.S. degree in electrical engineering from Hanyang University, Seoul, Korea, in 2021.

She is currently with HD Korea Shipbuilding and Offshore Engineering, where she is involved in the development of modular multilevel converter (MMC)-based propulsion drives, with a focus on hardware-in-the-loop simulation (HILS).

Shenghui Cui (Senior Member, IEEE) received the B.S. degree from Tsinghua University, Beijing, China, in 2012, the M.S. degree from Seoul National University, Seoul, South Korea, in 2014, and the Dr.-Ing. degree with the highest distinction (summa cum laude) from RWTH Aachen University, Aachen, Germany, in 2019, all in electrical engineering.

Since 2021, he is with Department of Electrical and Computer Engineering, Seoul National University, where he is currently an Associate Professor. From 2015 to 2021, he has been with the Institute for Power Generation and Storage Systems, E.ON Energy Research Center, RWTH Aachen University, where he worked as Research Associate and later on, Senior Scientist. His research interests include interaction of power systems and power converters, high-power converters in ac and dc utility applications (e.g., HVDC, FACTS, and SSTs), control and power hardware-in-the-loops, high-power ac drives for shipboard propulsions, and applications of wide-band gap power devices and cryogenic power electronics.

Dr. Cui was the recipient of the STAWAG Best Dissertation Prize from Faculty of Electrical Engineering and Information Technology, RWTH Aachen University in 2019, the Second Place Prize Paper Award of the IEEE Transactions on Power Electronics in 2018, and Best Paper Award of IEEE PEDG in 2025, the Second Prize Paper Award of IEEE IPEC (ECCE Asia) in 2018, and the Outstanding Presentation Award of the IEEE Applied Power Electronics Conference in 2014.